Algal blooms modulate organic matter remineralization in freshwater sediments: A new insight on priming effect

Algal blooms modulate organic matter remineralization in freshwater sediments: A new insight on priming effect

Yarui Wang,[a,b,c] Muhua Feng,[a,*] Jianjun Wang, [a] Xinfang Chen,[d] Xiangchao Chen,[a,c] Xian Du,[a] Fan Xun,[a,c] Bryne Tendelo Ngwenya[e]

[a]State Key Laboratory of Lake Science and Environment, Nanjing Institute of Geography and Limnology, Chinese Academy of Sciences, 73 Beijing East Road, Nanjing 210008, P. R. China

[b]Research Center for Eco-Environmental Sciences, Chinese Academy of Sciences, 18 Shuangqing Road, Beijing 100085, P. R. China

[c]University of Chinese Academy of Sciences, Beijing 100049, P. R. China

[d]Hydrology and Water Resources College, Hohai University, Nanjing 210098, P. R.China

[e] Microbial Geochemistry Laboratory, School of Geosciences, University of Edinburgh, EH9 3FE, UK

* Corresponding author. Muhua Feng, PhD.

E-mail: mhfeng@niglas.ac.cn;

Fax: +86 25 57714759;

Tel: +86 25 86882206

Abstract

This study provides a novel insight into the degradation of sediment organic matter (SOM) regulated by algae-derived organic matter (AOM) based on priming effect. We tracked the dynamics of SOM mineralization products and pathways, together with priming effects (PE) using the compound-specific stable isotope ($\delta^{13}C$) technique following addition of low- and high-density algal debris in sediments. We found that algal debris increased the total carbon oxidation rate, resulting in denitrification and methanogenesis-dominated SOM mineralization, while iron reduction and sulphate reduction played important roles in the early period of algal accumulation. Total carbon oxidation rate and anaerobic rates ($R_{anaerobic}$) were higher in the amended treatments compared with that in controls. Analysis indicated that algal debris had a positive PE on SOM mineralization, which resulted in an intensified mineralization in the initial phase with over 80% of dissolved inorganic carbon deriving from SOM degradation. Total carbon oxidation rate of SOM deduced from priming effect ($R_{TCOR\text{-}PE}$) was similar to $R_{anaerobic}$, further indicating SOM mineralization is a critical source of the end products. These findings deviate the causal focus from the decomposition of AOM, and confirm the accumulation of AOM as the facilitator of SOM mineralization. Our study offers empirical evidences to advance the traditional view on the effect of AOM on SOM mineralization.

Keywords: Algal debris accumulation; SOM mineralization; end products; endogenous contribution; priming effect

1. Introduction

Eutrophication is a major environmental issue of concern worldwide (Zhang et al., 2016; Plaas et al., 2021; Watson et al., 2021). It not only poses a threat to aquatic ecosystems with the release of toxic metabolites (Janssen, 2019; Jiang et al., 2014; Munoz et al., 2019; Olson et al., 2020), but also increases the intensity of algal debris settlement to sediment-water surfaces (Garcia-Robledo et al., 2008; Lee et al., 2016). Since sediments are both sources and sinks of organic and inorganic matters (e.g., nutrients, hydrogen sulfide (H_2S), iron (Fe), and methane (CH_4)), which are dependent on the redox environment (Shi et al., 2018; Tyler et al., 2003; Xu et al., 2015), algal debris increases have important implications for the behavior of these organic and inorganic components. The accumulation of algal detritus tends to modify and be involved in the biogeochemical cycle of Sedimentary Organic Matter (SOM) during algae-induced anoxia/hypoxia events (Garcia-Robledo et al., 2008; Karlson, 2008; Trevathan-Tackett et al., 2018; Tyler et al., 2003). Given that fresh algal-debris is bioavailable to microorganisms in aquatic environments due to its labile components (Pivokonsky et al., 2012; Zhou et al., 2019), both SOM and algal organic matter (AOM) are likely contributors to CO_2 production associated with nutrients loading of freshwater leading to algal blooms. For example, field monitoring and simulations have shown that the concentration of CO_2 and nutrients increases each summer during algal blooms (Shang et al., 2015; Zhu et al., 2020). Researchers have made efforts to identify the transportation and transformation behavior of nutrients between sediment and water

column during algal blooms, and a series of well-accepted theories have been established relating increase of nutrients loading to microbial activities and biodegradability of AOM (Andersen and Jensen, 1992; Finlay and Kendall, 2008; Lee et al., 2016; Mills and Alexander, 1974). Although these observations suggest a causal link between algae and nutrients, there are few direct evidences on the contribution of algae to SOM mineralization.

The term "priming effect" (PE), has been increasingly used in anaerobic systems to describe the phenomenon of refractory SOM remineralization, which has been recently linked to the decay of labile organic matter in marine ecosystems (Gontikaki et al., 2013; van Nugteren et al., 2009). This process is sometimes referred to as "cometabolism" (Wakeham and Canuel, 2006). In this case, a positive value represents the enhancement of SOM mineralization by labile organic matter, or vice versa, which is related to the sediment type and the quantity of added substrates (Gontikaki et al., 2013; Turnewitsch et al., 2007). Using stable isotope-labeled substrates (i.e., phytoplankton-derived material), van Nugteren et al. (2009) provided the convincing evidence that positive PE was found in intertidal and subtidal estuarine sediments. Therefore, when algal blooms happen, PE may potentially be an important indicator in evaluating the balance of carbon and nutrients in sediments.

Positive PE can facilitate carbon and nutrients cycling in sediments. Theoretically, the generation of carbon and nutrients is also proportionate to the utilization of terminal electron acceptors, primarily oxygen (O_2), nitrate (NO_3^-), hydrous maganese oxides (Mn-(hydr)oxides), Fe-(hydr)oxides, and sulfate (SO_4^{2-}) (Rozan et al., 2002; Thamdrup

and Canfield, 1996; Zhu et al., 2018). At the beginning of algal debris decay, notable changes have been observed with respect to SOM degradation reactions, often referred to as primary redox reactions (Canavan et al., 2006). For example, the decay of algal biomass can inhibit nitrification and thereby denitrification in sediments by depleting dissolved oxygen (Zhu et al., 2020). However, in the view of long-term accumulation of algal debris, this influence on denitrification or other SOM mineralization pathways may be different from that of the initial deposition phase. Importantly, understanding the contribution of SOM to end products provides novel opportunities to explore algal bloom mechanisms induced by nutrients loading in the future.

In this study, we investigated the effect of AOM on SOM mineralization in a sediment-water microcosms by combining the dynamic variation of nutrients, reduced species, and PE values. The primary motivation of this research was to determine the role of algal debris in SOM mineralization and to understand the SOM mineralization potential for widespread eutrophication arising from nutrients supply. Here, we sought to (1) determine the effects of algal detritus on the release of nutrients in sediment porewater, (2) evaluate the effect of algal detritus on the mineralization rates and the contributions of SOM mineralization pathways after long-term accumulation, (3) determine the magnitude and duration of the PE of algal detritus on SOM mineralization, and (4) develop a theoretical understanding of SOM mineralization supporting the supply of nutrients leading to algal blooms.

2. Materials and methods

2.1. Sediments and algal debris preparation

A total of nine intact sediment cores were collected using Plexiglas tubes (11 cm I.D., 50 cm long) in the center of the Yuqiao reservoir (N 40°02′7.29″, E 117°32′36.58″), in which the heights of sediment and overlying water were 30 and 19 cm, respectively. Yuqiao reservoir is located in Tianjin City, China, and plays an important role in supplying water for both industrial and household use in the nearby region. The surface area of Yuqiao reservoir is 135 km^2, with an average depth of 4.3 m (Wen et al., 2019; Cao et al., 2020). It is located in a humid continental climate with an average monthly temperature of 19±1 ℃ and an average annual rainfall of 748.5 mm. Eutrophication is evident from a large number of algae aggregate near the shore of the dam area, affected by wind, wind direction and other factors with a mean concentration of 50 μg L^{-1} of Chlorophyll-a (Chl-a). The water quality was affected by cyanobacterial blooms in summer and autumn in recent years. Algal samples were collected with the aid of a phytoplankton net (mesh size 64 microns). To obtain dried algal debris, cyanobacterial cells were rinsed several times with deionized water to exclude surface contamination, and centrifuged at 5000 r min^{-1} for 10 minutes to remove excess fluid and then freeze-dried (Moodley et al., 2000). The dried organic detritus was then scraped into a mortar and ground into powder. The characteristics of the sampled sediments and water were listed in Table S1.

130 *2.2. Sediment core incubations*

131

132 In order to simulate the deposition of algal debris on the sediment surface, three
133 experimental treatments were performed (Fig. 1a), including sediment only (i.e.,
134 unamended sediment as Control), algal debris amended once (i.e., ×1 amendment) and
135 amended 20 times (i.e., ×20 amendment). Each treatment was run in triplicate (n = 3).
136 Algal detritus biomass in the ×1 amendment and the ×20 amendment was equivalent to
137 6 and 120 g dw m^{-2}, representing the normal algal blooms level and black bloom
138 eruption level (e.g. the phenomenon of massive congregation of dead cyanobacteria) in
139 freshwaters, respectively (Wang et al., 2018a). Proteins, peptides, amino acids,
140 polysaccharides, oligosaccharides, lipids and various organic acids were the common
141 constituents of AOM, which were bioavailable to microorganisms in aquatic
142 environments (Pivokonsky et al., 2012; Zhou et al., 2019). The sediment columns were
143 incubated in the dark at the in-situ temperature of 16 ± 1 ºC. During incubation, 10 mL
144 of overlying water was sampled at approximately 10 mm above the sediment-water
145 interface for DO measurement with Unisense OX50 (Denmark), and was subsequently
146 filtered with a 0.45 μm filter for nutrient analyses at a given interval time. After each
147 sample collection, all cores were replenished with the original filtered water to
148 compensate for the sampling losses.

149

150 *2.3 Estimation of nutrient release fluxes from overlying water gradients*

151

152 During the sediment core incubations, the fluxes of nutrients at the sediment-water
153 interface were calculated by the following equation:

154 $$\boldsymbol{v = k \cdot V/A} \quad (1)$$

155 Where $\boldsymbol{v}$ represents the flux of dissolved matter (ie., ammonium (NH_4^+), nitrate
156 (NO_3^-) and dissolved oxygen (O_2)) at sediment-water interface (mmol m^{-2} d^{-1}); $\boldsymbol{k}$ is
157 determined by the linear regression of calibrated concentration ($\mathbf{C_n'}$) of NH_4^+ and NO_3^-
158 with time, mmol L^{-1} d^{-1}; $\mathbf{V}$ (L) is the overlying water volume, L; $\mathbf{A}$ (m^2) is the surface
159 area of the sediment column, m^2. DO consumption rate can be obtained by directly
160 using the Eq (1).

161 There was an equal supplementation of culture water to sediment core after per
162 interval sampling during sediment core incubations, the concentration of nutrients of
163 overlying water should be corrected according to Eq (2):

164 $$\mathbf{C_n' = C_n + \ (C_{n-1}' - C_0)\ \cdot V_0/V} \quad (2)$$

165 Where $\boldsymbol{C_n'}$ (mmol L^{-1}) is the corrected concentration of nutrients (NH_4^+ and
166 NO_3^-) at times n (≥2); $\boldsymbol{C_n}$ (mmol L^{-1}) is the overlying water concentration of nutrients
167 (NH_4^+ and NO_3^-) determined at times n (≥1); $\boldsymbol{C_0}$ (mmol L^{-1}) is the concentration of
168 nutrients (NH_4^+ and NO_3^-) of culture water; $\mathbf{V}$ (L) and $\mathbf{V_0}$ (L) are the overlying water
169 volume and the sampling volume respectively.

170

171 *2.4 Bag incubation and oxidation rates evaluation*

172

In view of the aging process of algal debris and sediments after core incubations, the mineralization of SOM in deeper sediments would be inevitably affected due to "bulk effect" with strongly anaerobic environment (Liu et al., 2014). Therefore, the effect was explored using polyethylene sealer (NEN/PE) bag incubations (Hansen et al., 2000). Briefly, after core incubations, each treatment was sectioned in a N_2-filled NEN/PE bag at 1- or 2-cm sediment interval down to 8 cm depth. Sections from the same depth were pooled, mixed, and loaded into gas-tight plastic bags to a final volume of 400−800 mL (Fig. 1b). These bags were further incubated in N_2-filled storage bags with 10 cm in length and width to further ensure anoxia and were sampled on days of 1, 10, 17, 29 and 42. All incubations were performed under the same condition as sediment core incubations.

Following Thomsen et al. (2004), sampling from each bag was initiated by subsampling 3 ml sediments and the sediment was quickly transferred to a 20 mL serum bottle which had been purged with N_2 for 1 min. The bottles were stoppered with a butyl rubber septum and crimped immediately. After 20 min shaking and standing, the diffusion of CH_4 in sediments can reach equilibrium with the headspace in the bottle (Nüsslein et al., 2001; Abe et al., 2005, 2010), which can represent the CH_4 generation capacity of the sediment on the sampling days. Then, CH_4 determination was performed on a gas chromatograph immediately (GC7890, Agilent, USA). Finally, methanogenesis rate was derived from the Michaelis-Menten equation of CH_4 concentration with time (that is the 1st, 10th, 17th, 29th and 42nd day). Porewater and sediment samples were also subsampled from bags at the same time for analyzing DIC,

195 NH_4^+, NO_3^-, Fe^{2+}, SO_4^{2-}, CH_4, solid phase Fe and excitation–emission matrices (EEMs)
196 tracing the composition of dissolved organic matter (DOM). A description of the
197 sampling procedure in different treatments and chemical analyses given in Supporting
198 Information.

199 The rates of DIC accumulation, NH_4^+-N accumulation, iron reduction (*R(Fe)*), and
200 sulfate reduction (*SRR*) were also derived from the Michaelis-Menten equation with the
201 time-series concentrations of DIC, NH_4^+-N, Fe^{2+}, and SO_4^{2-} in the porewater,
202 respectively (Liu et al., 2020). Denitrification rate ($R(NO_3^-)$) was determined at each
203 sampling day by the ^{15}N-tracer technique (Hou et al., 2015; Song et al., 2013).

204 Total carbon oxidation rate (TCOR) was the sum of accumulation rates of DIC
205 and CH_4 of different interval sediments (Sobek et al., 2009; Sutton-Grier et al., 2011).
206 The depth-integrated rates of reduction processes were the sum of corresponding
207 reduction rates in each sediment profile during bag incubation (Hyun et al., 2007, 2009).
208 Through the stoichiometry of each reaction (i.e., SO_4^{2-} to organic carbon of 1:2, NO_3^-
209 to organic carbon of 4:5, Fe^{2+} to organic carbon of 4:1, CH_4 to organic carbon of 2:1)
210 (Randlett et al., 2015), the anaerobic rate ($R_{anaerobic}$) of SOM and the relative
211 contribution of microbial reduction to the fraction of SOM mineralized with electron
212 acceptors was obtained, where $R_{anaerobic}$ was calculated as Eq (3):

213 $$R_{anaerobic} = 1.25 \cdot R(NO_3^-) + 0.25 \cdot R\ (Fe\ (II)) + 2 \cdot SRR + 2 \cdot R(CH_4) \quad (3)$$

214

215 *2.5 Priming effect study*

216

217 *2.5.1 Preparation of labelled algal debris*

218

219 As a source of tracer and possible priming of OM, *Microcystis aeruginosa* were
220 cultured in BG11 (Liu et al., 2018) containing 30% ^{13}C-enriched bicarbonate (Sigma,
221 Germany) and were treated as described in previous studies (Moodley et al., 2000; van
222 Nugteren et al., 2009; Wert et al., 2014). Briefly, the algae were harvested during the
223 exponential growth phase (20−28 days). To remove the ^{13}C-bicarbonate, the algal
224 suspension was centrifuged three times at 5000 r min^{-1} for 10 minutes using 18 MΩ
225 deionized distilled water. The washed cells underwent three freeze/thaw cycles (-70/25
226 ℃) to induce cell lysis, and then were centrifuged again to discard the supernatant, and
227 then freeze-dried. This produced axenic algal-derived carbon was obtained with the
228 value of 28.9% δ^{13}C. The chemical characteristics of algal debris are listed in Table S1.

229

230 *2.5.2 PE experiments*

231

232 To explore the phenomenon of PE during algal debris accumulation on the
233 sediment surface, three treatments were performed in 2.5 L culture bottles (i.e., bottom
234 area, 125 cm^2) with two replicates for each. Sediment only treatment consisted of 100
235 mL of sediments (i.e., the surface of sediment cores). The additive amount of labeled
236 algal debris in the once-amended and ×20 amended was equivalent to 6 and 120 g dw
237 m^{-2} of wet sediment (ws), respectively. Finally, the bottom water (300 mL) was added
238 to all treatments and was purged for 20 min with high purity N_2 to induce anoxic

conditions followed by sealing the bottles. Each bottle was put in the constant temperature box (16 ± 1 ℃) and connected to a Picarro G2201i isotope ratio mass spectrometer (Picarro, Inc., Santa Clara, C. USA) for real-time determination of CH_4 and CO_2 (Fig. 1c). The pH and DO in overlying water were analyzed in real time during incubation by online meters (Mettler-Toledo, AG, Analytical, Schwerzenbach, Switzerland). Overlying water (9 mL) was sampled on the day of 0, 1, 3, 7, 14, and 17, and was filtered with a 0.45 μm cellulose acetate filter for the detection of the concentration of DIC, Fe^{2+} and the value of DI$\delta^{13}C$ (-10.89‰, background value).

2.5.3 Monitoring process of CH_4 and CO_2

The concentrations of CH_4 and CO_2 and the values of $\delta^{13}C$-CH_4 and $\delta^{13}C$-CO_2 of each treatment were determined for 5 minutes during one measurement cycle. During each measurement interval, the analyzer was purged with high purity nitrogen (>99 %) for 5 minutes to wash the system for accurate detection. More than twenty determination cycles could be obtained per day of each treatment. The CO_2-CH_4 simultaneous mode of Picarro G2201i analyzer which was used in the study has a 5 min-averaged precision of <0.16‰ for $\delta^{13}C$-CO_2 and <1.15‰ for $\delta^{13}C$-CH_4, respectively and the detection limit of 100 ppm for CO_2 and 1.8 ppm for CH_4, respectively. Finally, the instrument response signal could vary during the 5-minute measurement cycle but always achieved a stable phase for 2 minutes during the cycle. The average concentrations and the isotope values of CH_4 and CO_2 of each day were

calculated from these 2-minute stable phases. For the assessment of PE, more details of the $\sum CO_2$ concentration calculation derived from the PE were based on van Nugteren et al. (2009). Additional details regarding analytical methods are shown in Supporting Information.

2.6 Statistical analyses

Linear, and nonlinear fittings were conducted using origin Lab 9.0 software. All statistical calculations were performed using SPSS 22.0. One-way analysis of variance (ANOVA) was used to test the statistical significance of differences among different treatments. All statistical analyses were considered significant at $p < 0.05$.

3. Results

3.1 DO and nutrients fluxes from overlying water gradients

As shown in Table 1, the average consumption rate of DO in the ×20 amendment was significantly higher than that of the control ($p < 0.05$), resulting in an anoxic condition in the ×20 amendment on the 4th day during sediment core incubations. A high concentration of ammonium (NH_4^+) with the effluxes of 11.70 ± 2.81 and 1.83 ± 0.15 mmol m^{-2} d^{-1} were found in the ×20 and the ×1 amendment, respectively; thus the treatments acted as sources of NH_4^+ while the control acted as a sink of NH_4^+. NO_3^- in

283 overlying water was constantly consumed with an average flux of 3.81 ± 1.03 mmol
284 m^{-2} d^{-1} in the ×20 amendment which was 4.00 and 3.30 times as much as that in the
285 control and the ×1 amendment, respectively. The highest NH_4^+ flux in the overlying
286 water was found in the ×20 amendment among the three treatments, which was
287 consistent with high NH_4^+ accumulation rates during bag incubation (Table S2).
288
289 *3.2 Characterization of dissolved organic matter.*
290
291 Five DOM components (C1-C5) were shown as obtained during the bag
292 incubation in Fig. S1 and Table S3. Moreover, the detailed characteristics of DOM were
293 described in Supporting Information. The contribution of total humic-like OM (C1, C3,
294 C4, and C5) was obviously higher than that of tryptophan-like (C2) OM in all
295 treatments (Fig. S2). The relative contributions of C1, C2, and C3 were decreased but
296 C4 and C5 increased over time (Fig. S2).
297
298 *3.3 Carbon mineralization*
299
300 As a result of the organotrophic microbial activity, DIC and NH_4^+ can be indicators
301 of the SOM degradation extent and the PE (Hannides and Aller, 2016). The
302 concentrations of DIC and NH_4^+ greatly increased over the incubation time and were
303 significantly higher in the ×20 amendment than that in other two treatments (Fig. 2).
304 The highest concentrations of DIC and NH_4^+ were found at the topmost layers with the

peak values of 9.38 and 2.33 mmol L^{-1}, respectively at the end incubation in the ×20 amendment. The accumulation rates of DIC in the pore water peaked at the topmost layer at 168.60 ± 2.76 μmol L^{-1} d^{-1} (in ×20) with intensive variation below 2 cm (Table S2). Higher total carbon oxidation rates were observed in the low and high densities of algal debris treatments compared to the control as shown in Table 2.

3.4 Anaerobic mineralization processes and rates

NO_3^- concentrations in the pore-water were below detection in the three treatments. The potential denitrification rate determined by a ^{15}N-tracer technique was highest at 1 cm with a value of 13.10 ± 0.84 μmol L^{-1} d^{-1} and then decreased to 6.90 ± 0.09 μmol L^{-1} d^{-1} below 1 cm in the control (Fig. 3a). The same vertical distribution was found in the ×20 amendment. In the ×1 amendment, the potential denitrification rate was highest at the bottom, with a value of 10.20 ± 0.09 μmol L^{-1} d^{-1}, followed by that in the surface sediment. Among the three treatments, the highest potential denitrification rates (8.50 ± 0.20 - 10.20 ± 0.09 μmol L^{-1} d^{-1}) were observed in the ×1 amendment except for that in the surface of the control.

The concentration of dissolved Fe^{2+} in the control was higher than that of the amended treatments, with the average values of 2.89 μmol·L^{-1} at the first day of bag incubations (Fig. 4a). However, Fe^{2+} concentration in the overlying water was highest in the ×20 amendment before 3 days during PE study (Fig. S3a). The total Fe was dominated by Fe (II) (Fig. 4d, f). For the Fe reduction rate, above 2 cm, higher rates

were found in the amended treatments compared with the control (Fig. 3b). Below the 2 cm, there is a similar behaviour between the ×20 amendment and the ×1 amendment (Fig. 3b).

The SO_4^{2-} concentrations, and the SRR were lowest in the ×20 amendment (Fig. 3c, 4b). The two parameters showed similar characteristics among all treatments; both were highest in the top 1 cm of sediment and then gradually decreased with depth. The depth-integrated rates of sulfate reduction were independent of the biomass of added organic matter, with the values of 17.67 ± 1.80, 16.69 ± 0.41 and 5.86 ± 0.61 nmol cm^{-2} d^{-1} in the control, ×1 amendment, and ×20 amendment, respectively (Table 2).

At the sediment surface, the CH_4 concentration in the ×20 treated amendment was slightly higher than that in the other two treatments (Fig. 4c), and decreased with depth but increased sharply below 4 cm. The reverse vertical distribution was found in the control. CH_4 concentration in the ×1 amendment of each depth was the lowest among the three treatments. Methanogenesis rate in the ×20 amendment at a depth of 0–1 cm was the lowest among the three treatments but increased sharply to the highest rate of 9.17 ± 1.17 μmol L^{-1} d^{-1} in the bottom sediment (Fig. 3d). The depth-integrated methanogenesis rates were 14.17 ± 2.00, 13.52 ± 1.79 and 27.89 ± 1.24 nmol cm^{-2} d^{-1} in the control, the ×1 and the ×20 amendments, respectively (Table 2).

3.5 Priming effect

The combined use of carbon isotopes in $\delta^{13}C$-CO_2, $\delta^{13}C$-DIC and $\delta^{13}C$-CH_4 can

elucidate the extent of organic matter degradation (Du et al., 2020). As shown in Fig. 5a and 5b, the $\delta^{13}C$-CO_2 and $\delta^{13}C$-CH_4 values (No data at day 0 due to zero or negligible CH_4 and CO_2 concentration) in the x20 amendment were higher compared with that of the x1 amendment. Algal debris addition indeed enhanced the release of $\sum CO_2$, but the contents of $\sum CO_2$ were independent of the amount of algal carbon added (Fig. 5c, Fig. 6a). The production of CH_4 was minimal initially but increased rapidly after a lag period of 10 days in the x20 amendment (Fig. 5d). There was little CH_4 (<0.1 ppm) release in the x1 amendment. On the other hand, DIC was a primary end product which was another form of CO_2 before diffusing to the atmosphere. The enrichment of $\delta^{13}C$-DIC values were observed in the x20 amendment compared with that of the x1 amendment and control, despite similar DIC concentrations in the two amended treatments (Table 4).

The pronounced difference in sediments carbon content influenced sediments organic carbon mineralization rate (the sum of DIC and CH_4 produced). TCORs in the ×1 amendment and ×20 amendment were higher than that of control during the incubation periods, respectively (Fig. 6a). There was an average of 6% ± 1.59% $\sum CO_2$ originating from the algal debris in the ×1 amendment (Table 3). Therefore, the rest of the $\sum CO_2$ excess fluxes (88% ± 3.0%) compared with the control potentially originated from the priming responses. For the ×20 amendment, an average 9% ± 1.46% of $\sum CO_2$ was from algal debris degradation (Table 3). The highest PE was found in the ×1 amendment, and the PE was equivalent to 2.90–5.00 times the mineralization content of control (Fig. 6b). PE was always positive before the 17th day in the x1 amendment

371 and ×20 amendment (Fig. 6b).

372

373 **4. DISCUSSION**

374

375 *4.1 Impacts of algal debris on carbon mineralization.*

376

377 Oxygen depletion by microbial degradation of the sinking algal debris induced
378 hypoxia/anoxia (Table 1). The redox potential in sediment can also be greatly decreased
379 after algal decay and result in strong reducing environments in quiet water (Liu et al.,
380 2014). With favorable conditions for strongly anaerobic microbial activities in the
381 whole sediment, it was reasonable that higher DIC and NH_4^+ concentrations were found
382 in the amended treatments (Fig. 2). The observed higher concentration profiles of NH_4^+
383 and DIC in the amendments indicated that the mineralization rates, such as those found
384 in marine sediments, were determined by the concentration and reactivity of the OM
385 (Muller et al., 2003; Petranich et al., 2018). Subsequently, higher TCORs of sediments
386 in the amended treatments were found in the study (Table 2). The lowest DIC to NH_4^+
387 (C/N) ratio of each interval sediment was observed in the ×20 amendment, ranging
388 from 3.26 to 7.47, compared with 6.97 to 28.12 in the ×1 amendment and 8.07 to 15.77
389 in the control, respectively (Fig. S4). This further indicated labile AOM was available
390 for anaerobic degradation and could facilitate the SOM mineralization. DOM is the
391 intermediate product of OM mineralization that can substantially exist in an anoxic
392 environment (Yang et al., 2014; Zhou et al., 2019). A high humic-like component (>

80%) was also observed in all treatments (Fig. S2) which also indicated the difficulty of DOM degradation by microbial activities. The main cause might be that DOM have been mineralized early wherein labile algal DOM such as tryptophan-like substances were consumed rapidly, leaving dominantly humic-like components (Wang et al., 2018b).

4.2 Impacts of algal debris on SOM mineralization.

The activities of denitrifiers were enhanced by AOM immediately after algal debris accumulation, followed by the rapid consumption of NO_3^- (Table 1). By exploring the potential denitrification rate of sediments, we found that there were different denitrification intensities in sediments affected by the accumulation of algal debris. Low density algal debris in sediment has been known to benefit the anaerobic metabolism of microbes in the ×1 amendment with higher denitrification rate (Fig. 3a), with the relatively high contribution of denitrification (i.e., 55%) to SOM mineralization in the control. The denitrification rate was the lowest in the ×20 amendment and the NH_4^+ accumulate rapidly (Fig. 2b, 3a). We suggested that algal accumulations in shallow lakes might cause negative impacts on nitrogen removal and make more nutrients available for algal proliferation. Similarly, it has been reported that the excessive algal biomass > 150 ug L^{-1} Chl-a can decrease the amount of nitrifiers and denitrifiers (Zhu et al., 2020). Hence, this study proved the "double-side effect" of

AOM on the denitrification process in sediment which played a critical role in the nitrogen cycle.

In the presence of algal biomass, the iron reduction rate was inhibited in the top 2 cm of sediments compared with the control (Fig. 3b). We assumed that iron reduction had intensively occurred immediately after the addition of algal debris, which resulted in minimum contribution to total carbon oxidation (Table 2). The reasons for this assumption as follow: 1) the PE experiment showed that the Fe^{2+} concentration in the overlying water increased within 2 days after algal debris addition (Fig. S3a), indicating that a rapid microbial reworking of autochthonous bio-labile AOM (within 48 h) likely fueled the accumulation of Fe^{2+} through iron reduction; 2) significant iron reduction was dependent on the presence of poorly crystalized Fe (III) (Thomsen et al., 2004). The inventory of Fe^{3+}, Fe^{2+} and total Fe in sediment was below 175 μmol g^{-1} ws in the amendment (Fig. 4d-f) and could not, therefore, efficiently out-compete sulfate reduction or methanogenesis in freshwater or marine sediments (Hyun et al., 2007; Hyun et al., 2009).

In the present study, the lowest SO_4^{2-} concentration in the porewater was found in the ×20 amendment, verifying that the microbial sulfate reduction process was enhanced by the initial addition of high density algal debris (Tang et al., 2019). The sulfide could react with Fe (II) to form iron-sulfide precipitates (FeS or FeS_2 (pyrite)) (Tang et al., 2019), potentially reducing Fe (II) concentration in water and sediments (Fig. 4a and d). Accordingly, the concentration of Fe^{2+} in the overlying water and porewater reduced sharply after 3 days in the PE experiment (Fig. S3a, b), which also

436 confirmed the intense sulfate and iron reduction activities during early degradation of
437 algal debris. However, the activity of sulfur reducing bacteria can be inhibited within 4
438 mmol L^{-1} of SO_4^{2-} (Jordan et al., 2008). The highest SRR was observed in the ×1
439 amendment contributing 20% to the total carbon oxidation, while sulfate reduction was
440 not a likely candidate (contributed 5% to TCOR) in the ×20 amendment (Table 2). SO_4^{2-}
441 was strongly depleted to a stable background level at early addition of AOM, and,
442 during the incubations, DIC production was not balanced by sulfate consumption in the
443 ×20 amendment (Fig. 4b, Table 2). To sum up, long-term bag incubations showed that
444 early-aged algal debris accelerated SO_4^{2-} consumption and reduced Fe^{2+} accumulation
445 in pore water (Fig. 4a, b). These observations suggested that SOM mineralization might
446 be dominated by different anaerobic pathways at different periods following
447 accumulation of algal debris.

448 Low density algal debris addition as ×1 amendment did not lead to CH_4 generation
449 (Fig. 4c, 5d). However, higher CH_4 concentrations were observed in the early stage
450 addition of higher algal biomass (Fig. 5d). The ebullition of CH_4 was also noticed in
451 the ×20 amendment during core incubations and the release rate of CH_4 was enhanced
452 with values ranging from 0.11 to 5.66 nmol m^{-2} s^{-1} (data not shown). This phenomenon
453 was weakened after long term accumulation, with 24% contribution to total carbon
454 oxidation in the ×20 amendment (Table 2). We speculated that the labile AOM fraction
455 might be responsible for the CH_4 ebullition (Borges et al., 2015), and CH_4 ebullition in
456 shallow-lake mesocosms was shaped by the deposition of algal debris.
457

458 *4.3. Possible interaction of PE and mineralization pathways.*

459

460 TCORs were enhanced during long term accumulation of algal biomass (Table 2),
461 especially during the early stages of biomass addition (Fig. 6a). To clarify the priming
462 effect of AOM on SOM, the values of δ^{13}C-DIC and δ^{13}C-CO_2, the concentrations of
463 DIC and CO_2 were studied systematically (Fig. 5). Previous studies showed that δ^{13}C-
464 CO_2 and δ^{13}C-CH_4 values were negative because of their natural source (Laskar et al.,
465 2016; Hartmann et al., 2020; Yacovitch et al., 2020). However, *Microcystis aeruginosa*
466 was labelled with $NaH^{13}CO_3$ (30% of total DIC) before incubation, thus, higher δ^{13}C-
467 CO_2 and δ^{13}C-CH_4 values were observed in the x20 amendment (Fig. 5a and b). This
468 observation also agreed with the recent investigations involving algae-labelled by δ^{13}C,
469 where δ^{13}C-CO_2 and δ^{13}C-CH_4 were highly positive during oxic/ anoxic environment
470 (Blair et al., 1996; Moodley et al., 2005; Hartmann et al. 2020). Compared with x20
471 amendment, higher concentration of $\sum CO_2$ and lower δ^{13}C-$\sum CO_2$ value in the x1
472 amendment indicated that $\sum CO_2$ might be largely from SOM mineralization.
473 Consistently, PE value also indicated that a minor addition of fresh OM (×1 amendment)
474 could induce SOM remineralization with higher PE value at early accumulation periods
475 of algal debris, and the positive PE of AOM on SOM lasted for 17 days (Fig. 6b). To
476 prove this, the TCOR of SOM evaluated by PE contribution ($R_{TCOR\text{-}PE}$) and the
477 anaerobic degradation rates of SOM assessed by different acceptors ($R_{anaerobic}$) were
478 compared. As shown in Table 2, in the ×1 amendment, the value of $R_{anaerobic}$ of SOM
479 mineralization was 146.05 ± 4.50 nmol cm^{-2} d^{-1}, which was close to $R_{TCOR\text{-}PE}$ value

480 (148.07 ± 25.09 nmol cm^{-2} d^{-1}) (Table 2). However, the value of $R_{TCOR-PE}$ was close to
481 but still higher than $R_{anaerobic}$ in the x20 amendment. The reason might be that the
482 depletion of Fe (III) and SO_4^{2-} after algal debris addition lowered the $R_{anaerobic}$ in the
483 x20 amendment. Whatever the cause, this confirmed that the use of PE data to calculate
484 of the mineralization rate of total carbon could reveal the actual SOM mineralization
485 rate and distinguish the relative contributions of SOM mineralization and AOM
486 degradation. The release of terminal products such as DIC and nutrients were largely
487 from the mineralization of the SOM, not the decomposition of AOM. Hence, this study
488 modified the present views that nutrient release largely resulted from algal blooms in
489 eutrophic lakes. That is to say, algal debris long-term accumulation could indeed
490 facilitate SOM as an important endogenous source. To the best of our knowledge, this
491 is the first study to simultaneously track the dynamic processes of DIC, nutrients, and
492 PE. This study provides new insights into the transformation rules of AOM and SOM
493 in shallow eutrophic reservoir/lakes.
494

495 ## 5. Conclusions

496

497 The present study showed that the accumulation of algal debris increased DIC and
498 nutrients emissions in the sediments. The mineralization rates of SOM in the low and
499 high density algal debris treatments were 1.23 and 1.91 times higher than that of the
500 control, respectively. High load of algal debris could induce $\sum CO_2$ and CH_4 emission
501 and rapidly consume other electro acceptors, resulting in denitrification dominanted

SOM mineralization. Consistenly, the PE results indicated the potential positive priming effect of AOM on SOM, where the addition of algal debris increased CO_2 production by 6 folds in the x20 amendment, with more than 84% coming from SOM degradation. Herein, the existence of PE has been successfully demonstrated by the release of DIC and nutrients mainly from the mineralization of the endogenous SOM. The combination of PE and anaerobic mineralization pathways in this study provides a new insight into the effects of algal debris on SOM mineralization.

Supporting Information.

The Supporting Information includes the estimation of nutrients fluxes from overlying water gradients, a description of sampling processes and quantification of the rates of anaerobic pathways, preparation of labeled algal debris, analysis of PE, details regarding analytical methods, characterization of dissolved organic matter and other additional data.

Notes

The authors declare no competing financial interest.

Acknowledgment

This work was supported by grants from National Natural Science Foundation of China (41877482 and 41471075), and Major Science and Technology Program for Water Pollution Control and Treatment of China (2017ZX07203-003 and 2017ZX07603-005). The authors thank for Yue Shen for the data collection and formal analysis.

References

Abe, D.S., Adams, D.D., Sidagis-Galli, C., Sikar, E., Tundisi, J.G. 2005. Sediment greenhouse gases (CH_4 and CO_2) in the Lobo-Broa Reservoir, São Paulo State, Brazil: Concentration sand diffuse Emission fluxes for carbon budget considerations. Lakes & Reservoirs Research and Management, 10, 201-209.

Abe et al., 2010, GHG Measurement Guidelines for Freshwater Reservoirs, The International Hydropower Association (IHA).

Andersen, F.O., Jensen, H.S., 1992. Regeneration of inorganic phosphorous and nitrogen from decomposition of seston in a fresh-water sediment. Hydrobiologia, 228, 71-81.

Blair, N.E., Levin, L.A., DeMaster, D.J., Plaia, G., 1996. The short-term fate of fresh algal carbon in continental slope sediments, Limnol. Oceanogr. 41(6):1208-1219.

Borges, A.V., Darchambeau, F., Teodoru, C.R., Marwick, T.R., Tamooh, F., Geeraert, N., Omengo, F.O., Guerin, F., Lambert, T., Morana, C., Okuku, E., Bouillon, S., 2015. Globally significant greenhouse-gas emissions from African inland waters. Nat. Geosci. 8(8), 637-642.

Canavan, R.W., Slomp, C.P., Jourabchi, P., Van Cappellen, P., Laverman, A.M., van den Berg, G.A., 2006. Organic matter mineralization in sediment of a coastal freshwater lake and response to salinization. Geochim. Cosmochim. Acta, 70(11), 2836-2855.

544 Cao, H., Han, L., Li, W., Liu, Z., Li, L., 2020. Inversion and distribution of total
545 suspended matter in water based on remote sensing images-A case study on
546 Yuqiao Reservoir, China. Water Eniron. Res. 99(4)582-595.
547 Du, Y., Deng, Y., Ma, T., Xu, Y., Wang, Y. X., 2020. Enrichment of Geogenic
548 Ammonium in Quaternary Alluvial-Lacustrine Aquifer Systems: Evidence from
549 Carbon Isotopes and DOM Characteristics. Environ. Sci. Technol. 54, 6104-6114.
550 Finlay, J.C., Kendall, C., 2008. Stable Isotope Tracing of Temporal and Spatial
551 Variability in Organic Matter Sources to Freshwater Ecosystems. Emerg. Med. J.
552 26, 183-186.
553 Garcia-Robledo, E., Corzo, A., de Lomas, J.G., van Bergeijk, S.A., 2008.
554 Biogeochemical effects of macroalgal decomposition on intertidal
555 microbenthos: a microcosm experiment. Mar. Ecol. Prog. Ser. 356, 139-151.
556 Gontikaki, E., Thornton, B., Huvenne, V.A.I., Witte, U., 2013. Negative Priming Effect
557 on Organic Matter Mineralisation in NE Atlantic Slope Sediments. Plos One
558 8(6): e67722.
559 Hannides, A.K., Aller, R.C., 2016. Priming effect of benthic gastropod mucus on
560 sedimentary organic matter remineralization. Limnol. Oceanogr. 61(5), 1640-
561 1650.
562 Hansen, J.W., Thamdrup, B., Jorgensen, B.B., 2000. Anoxic incubation of sediment in
563 gas-tight plastic bags: a method for biogeochemical process studies. Mar. Ecol.
564 Prog. Ser. 208, 273-282.

565 Hartmann, J.F., Gunthel, M., Klintzsch, T., Kirillin, G., Grossart, H.P., Keppler, F.,
566 Isenbeck-Schroter, M., 2020, High Spatiotemporal Dynamics of Methane
567 Production and Emission in Oxic Surface Water, Environ. Sci. Technol. 54(3),
568 1451-1463.
569 Hou, L., Yin, G., Liu, M., Zhou, J., Zheng, Y., Gao, J., Zong, H., Yang, Y., Gao, L.,
570 Tong, C., 2015. Effects of Sulfamethazine on Denitrification and the Associated
571 N_2O Release in Estuarine and Coastal Sediments. Environ. Sci. Technol. 49(1),
572 326-333.
573 Hyun, J.-H., Smith, A.C., Kostka, J.E., 2007. Relative contributions of sulfate- and
574 iron(III) reduction to organic matter mineralization and process controls in
575 contrasting habitats of the Georgia saltmarsh. Appl. Geochem. 22(12), 2637-2651.
576 Hyun, J.-H., Mok, J.-S., Cho, H.-Y., Kim, S.-H., Lee, K.S., Kostka, J.E., 2009. Rapid
577 organic matter mineralization coupled to iron cycling in intertidal mud flats of the
578 Han River estuary, Yellow Sea. Biogeochemistry. 92(3), 231-245.
579 Janssen, E.M.L., 2019. Cyanobacterial peptides beyond microcystins-A review on co-
580 occurrence, toxicity, and challenges for risk assessment. Water Res. 151, 488-499.
581 Jiang, W., Chen, L., Batchu, S.R., Gardinali, P.R., Jasa, L., Marsalek, B., Zboril, R.,
582 Dionysiou, D.D., O'Shea, K.E., Sharma, V.K., 2014. Oxidation of Microcystin-
583 LR by Ferrate(VI): Kinetics, Degradation Pathways, and Toxicity Assessments.
584 Environ. Sci. Technol. 48(20), 12164-12172.

585 Jordan, T.E., Cornwell, J.C., Boynton, W.R., Anderson, J.T., 2008. Changes in
586 phosphorus biogeochemistry along an estuarine salinity gradient: the iron
587 conveyer belt. Limnol. Oceanogr. 53(1), 172-184.
588 Karlson, A.M.L., 2008. Benthic-pelagic coupling in the northern Baltic Sea: the link
589 between settling cyanobacterial blooms and macrobenthos. Ecology.
590 Laskar, A.H., Mahata, S., Liang, M.C., 2016, Identification of Anthropogenic CO_2
591 Using Triple Oxygen and Clumped Isotopes, Environ. Sci. Technol.
592 50(21),11806-11814.
593 Lee, Y., Lee, B., Hur, J., Min, J.-O., Ha, S.-Y., Ra, K., Kim, K.-T., Shin, K.-H., 2016.
594 Biodegradability of algal-derived organic matter in a large artificial lake by using
595 stable isotope tracers. Environ. Sci. Pollut. R. 23(9), 8358-8366.
596 Liu, B., Qu, F.S., Yu, H.R., Tian, J.Y., Chen, W., Liang, H., Li, G.B., Van der Bruggen,
597 B ., 2018. Membrane Fouling and Rejection of Organics during Algae-Laden
598 Water Treatment Using Ultrafiltration: A Comparison between in Situ
599 Pretreatment with Fe(II)/Persulfate and Ozone. Environ. Sci. Technol. 52(2) 756-
600 774.
601 Liu, G.F., Fan, C.X., Zhang, L., Shen,Q.S., Wang, Z.D., 2014. Environment Effects of
602 Algae-Caused Black Spots: Driving Effects on the N, P Changes in the Water-
603 Sediment Interface. China Environmental Science; 000: 3199-3206.
604 Mills, A.L., Alexander, M., 1974. Microbial decomposition of species of freahwater
605 planktonic algae. J. Environ. Qual. 3, 423-428.

606 Moodley, L., Boschker, H.T.S., Middelburg, J.J., Pel, R., Herman, P.M.J., de Deckere,
607 E. and Heip, C.H.R., 2000. Ecological significance of benthic foraminifera: ^{13}C
608 labelling experiments. Mar. Ecol. Prog. Ser. 202, 289-295.
609 Moodley, L., Middelburg, J.J., Soetaert, K., Boschker, H.T.S., Herman, P.M.J., Heip,
610 C.H.R., 2005, Similar rapid response to phytodetritus deposition in shallow and
611 deep-sea sediments, J. Mar. Res. 63, 457-469.
612 Muller, B., Wang, Y., Dittrich, M., Wehrli, B., 2003. Influence of organic carbon
613 decomposition on calcite dissolution in surficial sediments of a freshwater lake.
614 Water Res. 37(18), 4524-4532.
615 Munoz, M., Nieto-Sandoval, J., Cires, S., de Pedro, Z.M., Quesada, A., Casas, J.A.,
616 2019. Degradation of widespread cyanotoxins with high impact in drinking water
617 (microcystins, cylindrospermopsin, anatoxin-a and saxitoxin) by CWPO. Water
618 Res. 163, 114853.
619 Nüsslein, B., Chin, K. J., Eckert, W., Conrad, R., 2001. Evidence for anaerobic
620 syntrophic acetate oxidation during methane production in the profundal sediment
621 ofsubtropical Lake Kinneret (Israel). Environ. Microbiol. 3(7), 460-470.
622 Olson, N.E., Cooke, M.E., Shi, J., Birbeck, J.A., Westrick, J.A., Ault, A.P., 2020.
623 Harmful Algal Bloom Toxins in Aerosol Generated from Inland Lake Water.
624 Environ. Sci. Technol. 54(8), 4769-4780.
625 Petranich, E., Covelli, S., Acquavita, A., De Vittor, C., Faganeli, J., Contin, M., 2018.
626 Benthic nutrient cycling at the sediment-water interface in a lagoon fish farming
627 system (northern Adriatic Sea, Italy). Sci. Total Environ. 644, 137-149.

628 Pivokonsky, M., Safarikova, J., Bubakova, P., Pivokonska, L., 2012. Coagulation of
629 peptides and proteins produced by Microcystis aeruginosa: Interaction
630 mechanisms and the effect of Fe-peptide/protein complexes formation. Water Res.
631 46(17), 5583-5590.
632 Plaas, H. E., Paerl, H. W., 2021. Toxic Cyanobacteria: A Growing Threat to Water and
633 Air Quality. Environ. Sci. Technol. 55(1), 44-64.
634 Randlett, M.-E., Sollberger, S., Del Sontro, T., Muller, B., Pablo Corella, J., Wehrli,
635 B., Schubert, C.J., 2015. Mineralization pathways of organic matter deposited in
636 a river-lake transition of the Rhone River Delta, Lake Geneva. Environ. Sci.-Proc.
637 & Imp. 17(2), 370-380.
638 Rozan, T.F., Taillefert, M., Trouwborst, R.E., Glazer, B.T., Ma, S.F., Herszage, J.,
639 Valdes, L.M., Price, K.S., Luther, G.W., 2002. Iron-sulfur-phosphorus cycling in
640 the sediments of a shallow coastal bay: Implications for sediment nutrient release
641 and benthic macroalgal blooms. Limnol. Oceanogr. 47(5), 1346-1354.
642 Shang, L., Feng, M., Liu, F., Xu, X., Ke, F., Chen, X., Li, W.C., 2015. The
643 establishment of preliminary safety threshold values for cyanobacteria based on
644 periodic variations in different microcystin congeners in Lake Chaohu, China.
645 Environ. Sci.: Proc. & Imp. 17: 728-739.
646 Shi, W., Pan, G., Chen, Q., Song, L.R., Zhu, L., Ji, X., 2018. Hypoxia Remediation and
647 Methane Emission Manipulation Using Surface Oxygen Nanobubbles. Environ.
648 Sci. Technol. 52(15), 8712-8717.

649 Song, G.D., Liu, S.M., Marchant, H., Kuypers, M.M.M., Lavik, G., 2013. Anammox,
650 denitrification and dissimilatory nitrate reduction to ammonium in the East China
651 Sea sediment. Biogeosciences. 10(11), 6851-6864.
652 Sobek, S., Durisch-Kaiser, E., Zurbruegg, R., Wongfun, N., Wessels, M., Pasche, N.,
653 Wehrli, B., 2009. Organic carbon burial efficiency in lake sediments controlled by
654 oxygen exposure time and sediment source. Limnol. Oceanogr. 54, 2243-2254.
655 Sutton-Grier, A.E., Keller, J.K., Koch, R., Gilmour, C., Megonigal, J.P., 2011. Electron
656 donors and acceptors influence anaerobic soil organic matter mineralization in
657 tidal marshes. Soil Biol. Biochem. 43, 1576-1583.
658 Tang, Y., Zhang, M., Sun, G. and Pan, G., 2019. Impact of eutrophication on arsenic
659 cycling in freshwaters. Water Res. 150, 191-199.
660 Thamdrup, B., Canfield, D.E., 1996. Pathways of carbon oxidation in continental
661 margin sediments off central Chile. Limnol. Oceanogr. 41(8), 1629-1650.
662 Thomsen, U., Thamdrup, B., Stahl, D.A., Canfield, D.E., 2004. Pathways of organic
663 carbon oxidation in a deep lacustrine sediment, Lake Michigan. Limnol.
664 Oceanogr. 49(6), 2046-2057.
665 Trevathan-Tackett, S.M., Thomson, A.C.G., Ralph, P.J., Macreadie, P.I., 2018. Fresh
666 carbon inputs to seagrass sediments induce variable microbial priming responses.
667 Sci. Total Environ. 621, 663-669.
668 Turnewitsch, R., Domeyer, B., Graf, G., 2007. Experimental evidence for an effect of
669 early-diagenetic interaction between labile and refractory marine sedimentary
670 organic matter on nitrogen dynamics. J. Sea Res. 57(4), 270-280.

671 Tyler, A.C., McGlathery, K.J., Anderson, I.C., 2003. Benthic algae control sediment-
672 water column fluxes of organic and inorganic nitrogen compounds in a
673 temperate lagoon. Limnol. Oceanogr. 48(6), 2125-2137.
674 van Nugteren, P.V., Moodley, L., Brummer, G.J., Heip, C.H.R., Herman, P.M.J.,
675 Middelburg, J.J.J.M.B., 2009. Seafloor ecosystem functioning: the importance
676 of organic matter priming. Mar. Biol. 156(11), 2277-2287.
677 Wakeham, S.G., Canuel, E.A., 2006. Degradation and preservation of organic matter
678 in marine sediments. Marine Organic Mattter: Biomarkers, Isotopes and DNA 2,
679 295-321.
680 Wang, Y., Chen, X., Fu, X., Zhong, J., Chen, K., Wang, C., Feng, M., 2018a. The
681 releasing characteristics of carbon, nitrogen and phosphorus from sediment
682 under the influence of different densities of algal detritus. Journal of Lake
683 Sciences. 04: 925-936.
684 Wang, Y., Chen, X., Chen, B., Zhong, J., Fan, K.E., Chen, K., Feng, M., 2018b. The
685 release of pollutants in sediment-water interface after algal-debris accumulated in
686 sediments. Acta Sci. Circum. 38(01), 142-153.
687 Watson, J. S., Megan, A. A., Wang, T., Si, B., Zhang, Y., 2021. Biocrude Oil from
688 Algal Bloom Microalgae: A Novel Integration of Biological and Thermochemical
689 Techniques. Environ. Sci. Technol. 55(3), 1973-1983.
690 Wen, S., Wu, T., Yang, J., Jiang, X., Zhong, J., 2019. Spatio-Temporal Variation in
691 Nutrient Profiles and Exchange Fluxes at the Sediment-Water Interface in Yuqiao
692 Reservoir, China. Int. J. Environ. Res. Public Health. 16(17).

693 Wert, E.C., Korak, J.A., Trenholm, R.A., Rosario-Ortiz, F.L., 2014. Effect of oxidant
694 exposure on the release of intracellular microcystin, MIB, and geosmin from three
695 cyanobacteria species. Water Res. 52, 251-259.
696 Xu, H., Paerl, H.W., Qin, B., Zhu, G., Hall, N.S., Wu, Y., 2015. Determining Critical
697 Nutrient Thresholds Needed to Control Harmful Cyanobacterial Blooms in
698 Eutrophic Lake Taihu, China. Environ. Sci. Technol. 49(2), 1051-1059.
699 Yacovitch, T.I., Daube, C., Herndon, S., 2020. Methane Emissions from Offshore Oil
700 and Gas Platforms in the Gulf of Mexico, Environ. Sci. Technol. 54(6), 3530-
701 3538.
702 Yang, L., Choi, J.H., Hur, J., 2014. Benthic flux of dissolved organic matter from lake
703 sediment at different redox conditions and the possible effects of biogeochemical
704 processes. Water Res. 61, 97-107.
705 Zhang, X., Deng, J., Xue, Y., Shi, G., Zhou, T., 2016. Stimulus Response of Au
706 NPs@GMP-Tb Core-Shell Nanoparticles: Toward Colorimetric and Fluorescent
707 Dual-Mode Sensing of Alkaline Phosphatase Activity in Algal Blooms of a
708 Freshwater Lake. Environ. Sci. Technol. 50(2), 847-855.
709 Zhou, Y., Zhou, L., Zhang, Y., de Souza, J.G., Podgorski, D.C., Spencer, R.G.M.,
710 Jeppesen, E., Davidson, T.A., 2019. Autochthonous dissolved organic matter
711 potentially fuels methane ebullition from experimental lakes. Water Res.166,
712 115048.
713 Zhu, L., Shi, W., Van Dam, B., Kong, L., Yu, J., Qin, B., 2020. Algal Accumulation
714 Decreases Sediment Nitrogen Removal by Uncoupling Nitrification-

715 denitrification in Shallow Eutrophic Lakes. Environ. Sci. Technol. 54(10), 6194-
716 6201.
717 Zhu, N., Wu, Y., Tang, J., Duan, P., Yao, L., Rene, E.R., Wong, P.K., An, T.,
718 Dionysiou, D.D., 2018. A New Concept of Promoting Nitrate Reduction in
719 Surface Waters: Simultaneous Supplement of Denitrifiers, Electron Donor Pool,
720 and Electron Mediators. Environ. Sci. Technol. 52(15), 8617-8626.

721

722 **Table 1.** Measured fluxes from sediment core incubations

723

Treatment	Parameters	Measured fluxes rate ± SE (*n*) (mmol m^{-2} d^{-1})
Control	O_2	-9.51 ± 0.22
	NH_4^+	-2.23 ± 0.21
	NO_3^-	-0.92 ± 0.41
×1 amendment	O_2	-10.31 ± 0.89*
	NH_4^+	1.83 ± 0.15**
	NO_3^-	-1.41 ± 0.32*
×20 amendment	O_2	-14.31 ± 2.31**
	NH_4^+	11.70 ± 2.81**
	NO_3^-	-3.81 ± 1.03**

724 One-way analysis of variance (ANOVA) is used to test the statistical significance of

725 differences of nutrients between amended treatments and control.

726 *, $p < 0.05$; **, $p < 0.01$.

727

728 **Table 2.** Depth-integrated rates of different anaerobic pathways, as well as TCOR and anaerobic degradation rates of SOM assessed by

729 different acceptors ($R_{anaerobic}$) during bag incubations. TCOR of SOM (0-8 cm) evaluated by PE contribution ($R_{TCOR\text{-}PE}$).

Treatment	Microbial process rate ($nmol \cdot cm^{-2} \cdot d^{-1}$)				TCOR[b] ($nmol \cdot cm^{-2} \cdot d^{-1}$)	$R_{anaerobic}$[c] ($nmol \cdot cm^{-2} \cdot d^{-1}$)	$R_{TCOR\text{-}PE}$[d] ($nmol \cdot cm^{-2} \cdot d^{-1}$)
	Denitrification	Iron reduction	Sulfate reduction	Methanogenesis		0-8 cm	0-8 cm
Control	59.56 ± 0.38	4.27 ± 0.18	17.67 ± 1.80	14.17 ± 2.00	136.10 ± 6.93	139.17 ± 6.58	--
% Total[a]	55	1	26	21			
×1 amendment	67.50 ± 0.22	5.01 ± 0.73	16.69 ± 0.41	13.52 ± 1.79	167.93 ± 7.83	146.05 ± 4.50	148.07 ± 25.09
% Total	50	1	20	16			
×20 amendment	56.26 ±0.18	6.46 ± 0.69	5.86± 0.61	27.89 ± 1.24	260.24 ± 8.27	139.42 ± 3.68	217.81 ± 8.79
% Total	27	1	4.5	24			

730

[a] "% Total" is the percentage of each microbial process to the total carbon oxidation; [b] TCOR was the sum of accumulation rates of DIC and CH_4 of different interval sediments; [c] $R_{anaerobic}$ was the sum of interval sediment $R_{anaerobic}$ according to the stoichiometric equations (Randlett et al., 2015); [d] $R_{TCOR\text{-}PE}$ is the product of TCOR and %(SOM), where %(SOM) was the contribution of SOM mineralization to TCOR evaluated from PE experiment.

734 **Table 3.** End $\sum CO_2$ concentration in the different treatments (mg L^{-1}) and the average
735 contribution of algal debris to carbon oxidation in the amended treatments under anoxic
736 conditions at the end of the experiment during PE experiments.

Treatment	End $\sum CO_2$ (mg L^{-1})	Average algal debris contribution (%)	$\delta^{13}C$ of $\sum CO_2$ produced (‰)	Maximum $\sum CO_2$ from C-dissolution (%)
Control	6.11	0	-49.95	3.61
×1 amendment	9.55	6.36 ± 1.59	3.12	3.61
×20 amendment	27.83	8.61 ± 1.46	464.33	3.61

737 Maximum dissolution was taken to be constant per given sediment and dissolution in amended
738 treatments, equal to corresponding control-background dissolution values. All values are average of
739 n = 3.

740 **Table 4.** The value of δ^{13}C-DIC and δ^{13}C-CO_2, and the concentration of DIC and CO_2

741 in the amended treatments during PE experiments.

742

Treatment	Time (days)	DIC (ppm)	δ^{13}C- DIC (‰)	CO_2 (ppm)	δ^{13}C-CO_2 (‰)
x1 amendment	1	1.51 ± 0.27	58.91	1.60 ± 0.64	-21.19 ± 3.20
	7	1.46 ± 0.42	48.78	29.91 ± 1.89	-17.71 ± 0.10
	14	1.62 ± 0.35	47.54	42.49 ± 0.34	-17.22 ± 0.12
	17	1.35 ± 0.12	43.21	37.91 ± 1.21	-16.05 ± 0.07
x20 amendment	1	1.42 ± 0.17	252.48	1.48 ± 1.02	67.14 ± 14.39
	7	1.91 ± 0.62	395.48	21.64 ± 0.97	306.78 ±9.30
	14	2.55 ± 0.19	400.39	29.80 ±0.66	400.12 ± 2.72
	17	2.19 ± 0.54	418.69	33.67 ± 1.04	422.5 ± 2.12

743

744

745 **Figure legends**

746 **Fig. 1.** Schematic diagram of experimental facility (a) core incubations; (b) bag
747 incubations; (c) The diagrammatic sketch of experimental devices.

748

749 **Fig. 2.** (a) The vertical distribution of DIC and (b) NH_4^+-N in the pore water of
750 sediments during the experiment. The error bars show the standard deviation (n = 3).

751

752 **Fig. 3.** Vertical distributions of (a) the denitrification rate, (b) the iron reduction
753 rate, (c) the sulfate reduction rate, and (d) the methanogenesis rate in the various
754 treatments during bag-incubation experiment. The error bars show the standard
755 deviation (n = 3).

756

757 **Fig. 4.** Vertical distributions of chemical compounds in liquid and solid phase at the
758 beginning of bag incubation in the different treatments. (a) Fe^{2+}, (b) SO_4^{2-}, (c) CH_4 in
759 pore water, (d) Fe (II), (e) Fe (III), and (f) total Fe in the solid phase during the bag-
760 incubation experiment. The error bars show the standard deviation (n = 3).

761

762 **Fig. 5.** The dynamic of $\delta^{13}C$-CO_2 (a) and $\delta^{13}C$-CH_4 (b); The concentrations of CO_2 (c)
763 and CH_4 (d) in the head space of different treatments during PE experiments. The error
764 bars show the standard deviation (n = 24).

765

766 **Fig. 6.** (a) The amount of ΣCO_2 mineralized after 7, 14, and 17 days of incubation in
767 background (Unamended) and amended (single and 20–fold load) sediment (n = 3)
768 during PE experiments; (b) Division of ΣCO_2 excess fluxes above unamended rates
769 between that from tracer algal organic matter (AOM) and that of sedimentary organic
770 matter (SOM) priming after 7, 14, and 17 days of the priming effect study. The error
771 bars show the standard deviation (n = 3).

772

773

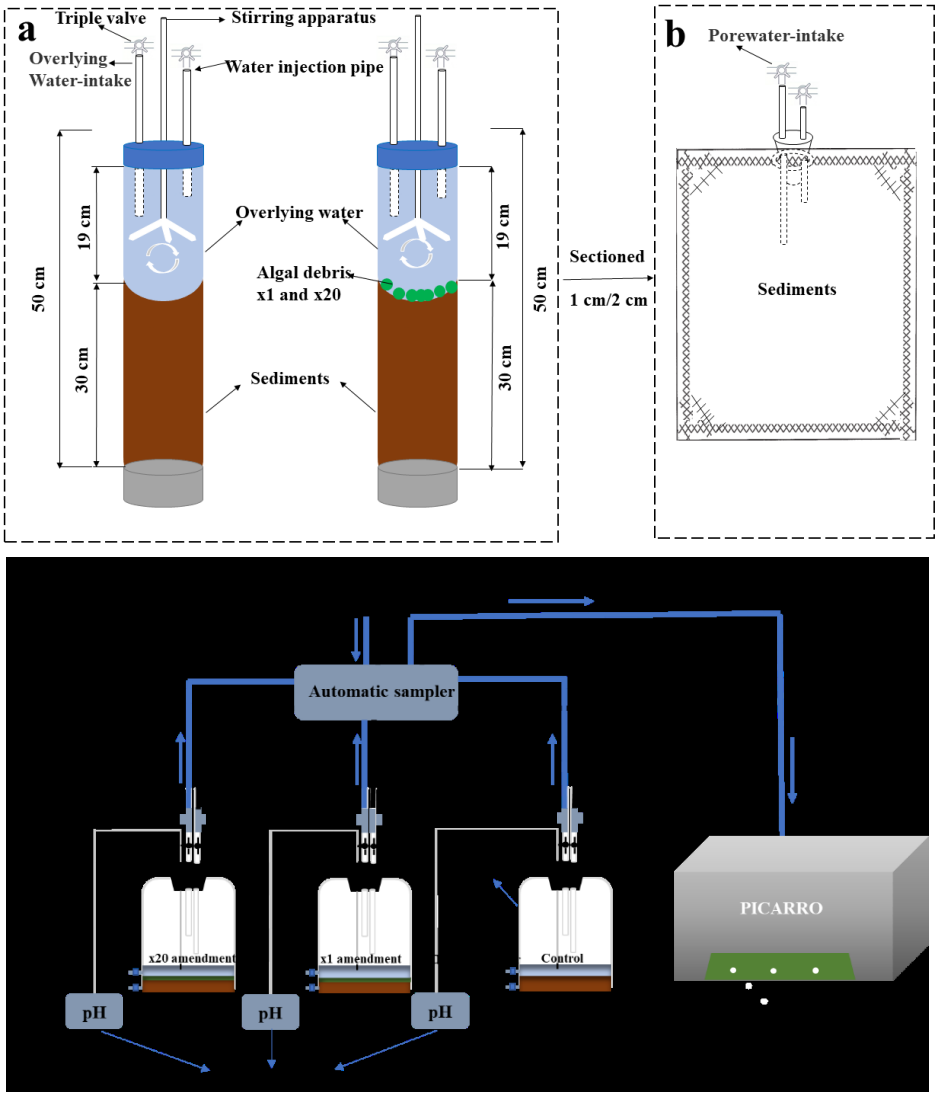

774

775 **Figure 1**

776

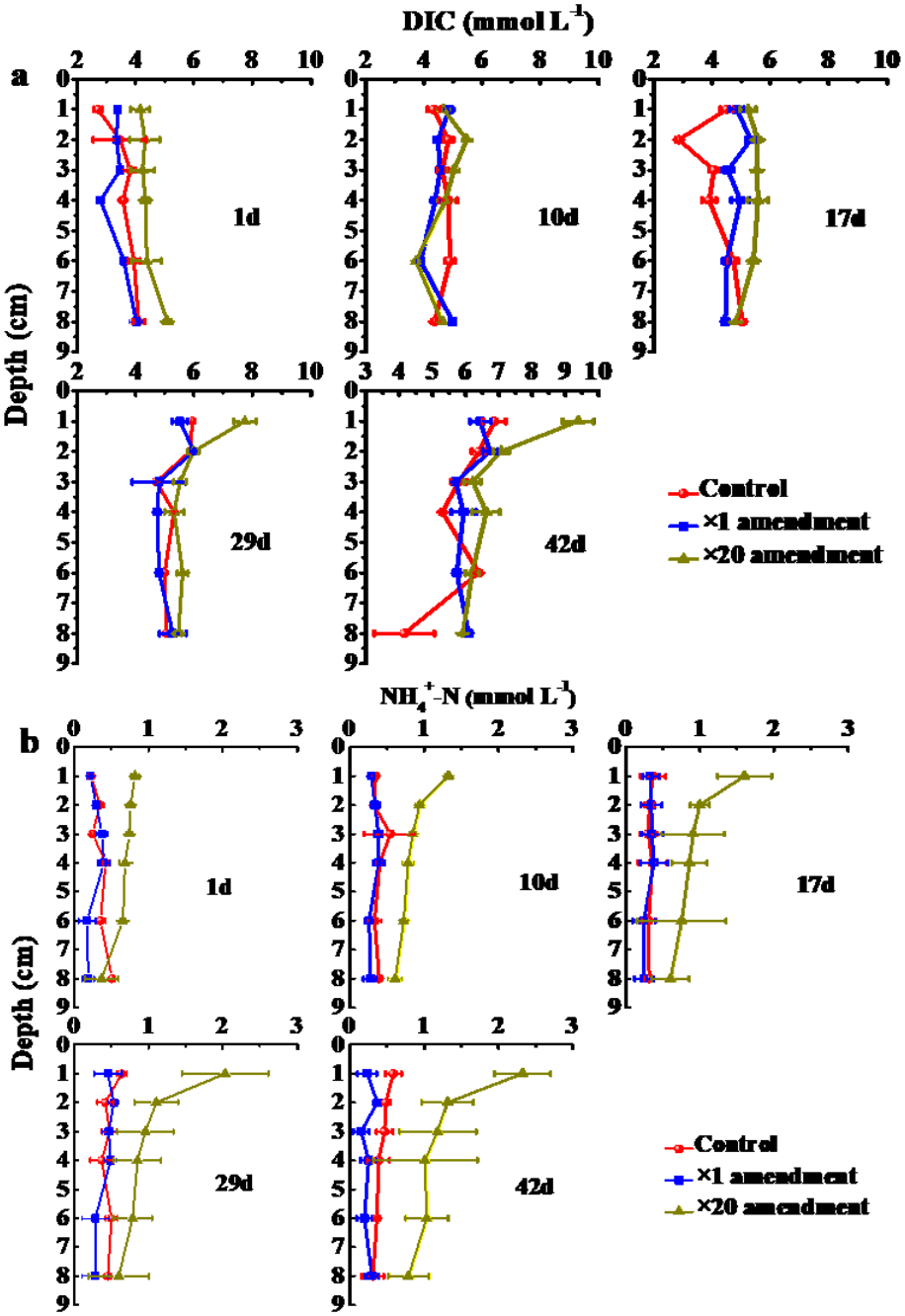

777

778

779 **Figure 2**

780

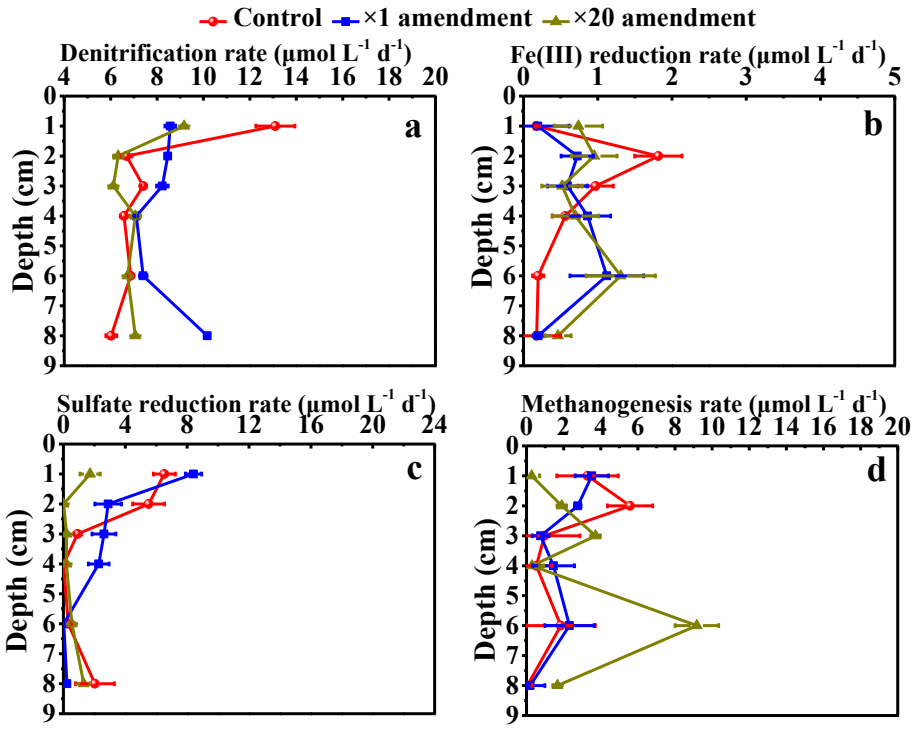

781

782

783 **Figure 3**

784

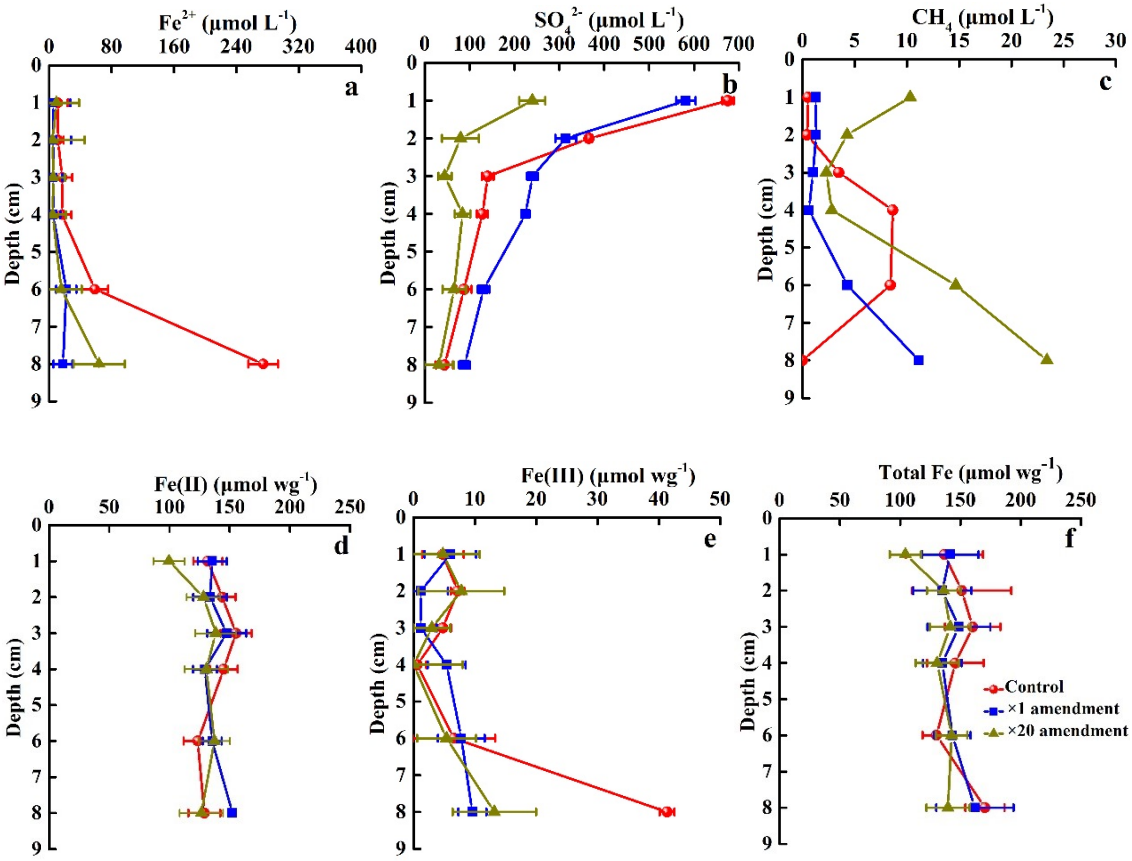

785

786 **Figure 4**

787

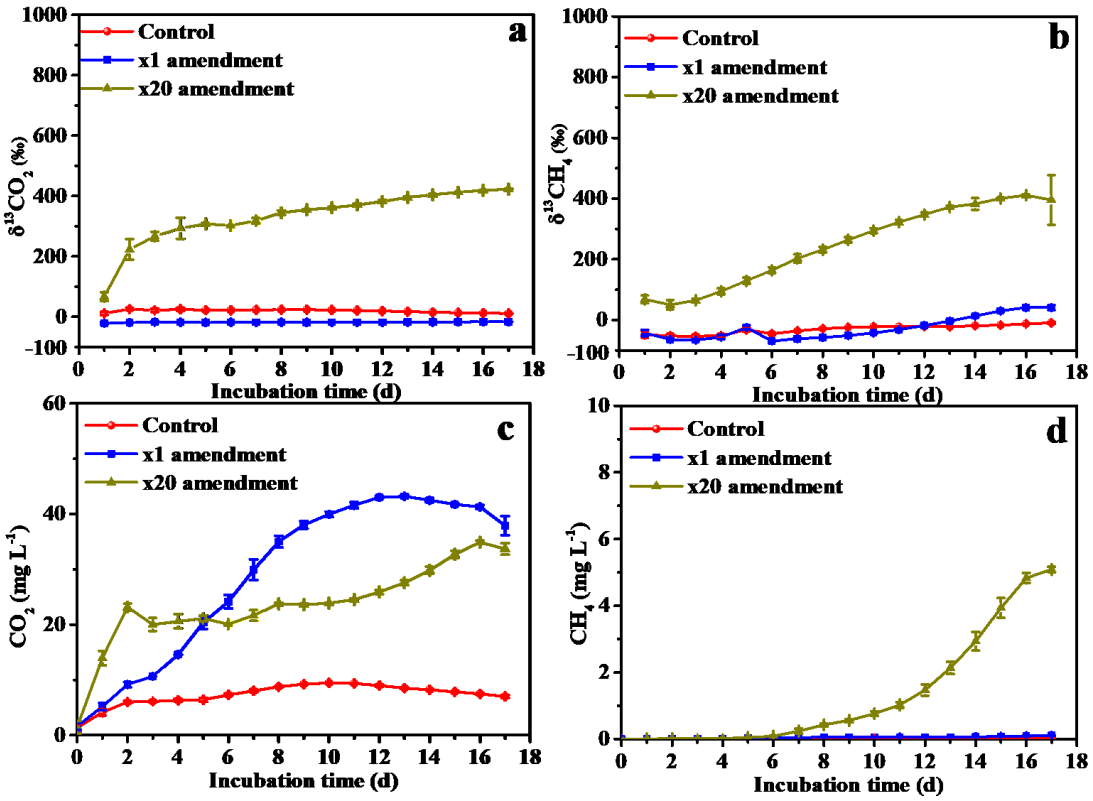

788

789

790 **Figure 5**

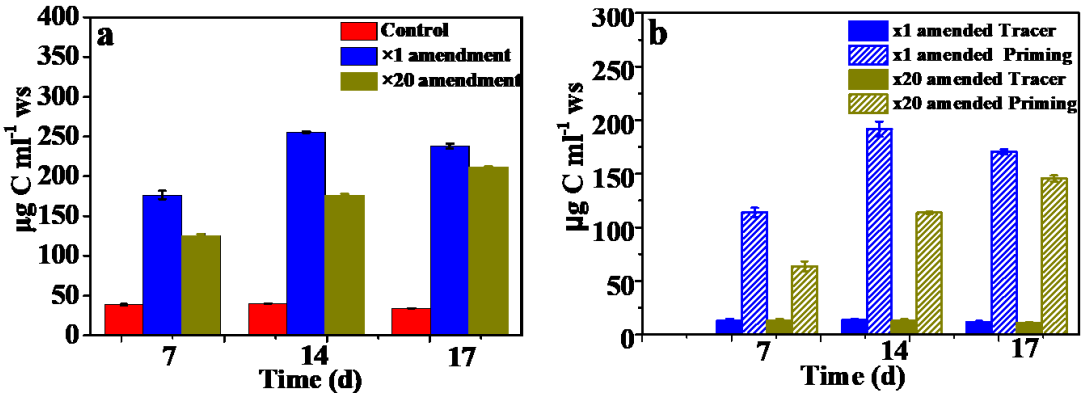

791

792 **Figure 6**

Supporting Information

Contents

Text S1 Description of sampling method

Samples of undisturbed surface sediments (0–30 cm) were collected using Plexiglas tubes sampler, and then were stored in sealed polyethylene barrels. The overlying water (25 L) was collected and filtered through pre-combusted GF/F filters for a subsequent incubation experiment and other analyses after detecting the water quality parameters with HACH Q40 (USA). The sediment cores were transported to the laboratory, and stored at in-situ temperature (16 ± 1 ^{o}C) within 12 hours from collection. The characteristics of the sediments and water is listed in **Table S1.**

At the beginning of the experiment, the overlying water was siphoned from each core. After the algal detritus was added to the sediment surface, the cores were carefully replaced with filtered bottom reservoir water.

Text S2 Description of sampling processes during bag incubations

In order to reveal the total carbon oxidation rate and the rates of denitrification, iron reduction, sulfate reduction, and methanogenesis, a specific sampling process was conducted as following. During bags incubations, firstly, sampling 50 mL sediment to two 50 mL centrifuge tubes respectively in each interval time, pore water was extracted with 2.5 OD Rhizons soil moisture samplers (Rhizosphere, Wagenigen, Holland) from

each layered sediment. Next, 5 mL porewater was filled with the 5 ml brown tube leaving no head space and was kept in 4 ^{o}C for the analysis of DIC next day. 5 mL porewater was determined for the concentration of Fe^{2+} within 1 h after sampling. Subsequently, 10 mL pore water was placed in a 15 mL centrifuge tube which were immediately frozen at -20 ^{o}C for later analysis of UV, EEMs, NO_3^- and NH_4^+. 5 mL pore water was placed in a 10 mL centrifuge tube, acidified with 6 mol L^{-1} HCl (1% vol), and stored for the later determination of SO_4^{2-}.

Denitrification rate (*R(NO_3^-)*) was determined at each sampling day by ^{15}N-tracer technique (Hou et al., 2015; Song et al., 2013). The process of determining denitrification rate was conducted in culture container vial (Labco, EK) as described by Song (2013) (Song et al., 2013). Briefly, 1.5 mL sediment sample was transferred to the vial and mixed with 10.5 mL He-degasses bottom water, stoppering by a plug for pre-incubation in the same condition as mentioned previously to run out NO_3^-. And then, 1.5 mL $Na^{15}NO_3$ solution was added to the tube to a final concentration of 100 μM after 10 h pre-incubation. In the following incubation time, vials were periodically shaken to ensure that labeled N was homogenously distributed and 5 subsamples were withdrawn during incubation. The sampling time series were 0, 2, 5, 9, and 24 h, with two parallels. At each sampling time, 0.5 mL $ZnCl_2$ (0.5 g mL^{-1}) solution was added to the designated tube to stop the activity of the microorganism. The vials added $ZnCl_2$ were stored in the condition (16 ± 1°C, dark) until subsequent N_2 isotope ratio analysis.

855 $^{29}N_2$, $^{30}N_2$, and O_2 in the culture solution were measured on a membrane interface mass
856 spectrometer (MIMS) (Kana et al., 1994).

857 For bulk sediment samples, 0.5 g sediments were taken at each sampling time for
858 the determination of solid phase Fe during bag incubations. The sediment was extracted
859 by adding 8 ml 0.5 M HCl solution and shaking for 1 h at room temperature, and then
860 centrifuged at 5000 rpm for 5 min. The supernatant was filtered by 0.45 μm cellulose
861 acetate filter to analyze total Fe, L-Fe (II), and Fe (III).

862

863 **Text S3 Details regarding analytical methods**

864

865 The concentration of NH_4^+ and NO_3^- were determined by Nessler's reagent
866 colorimetry and dual wavelength ultraviolet spectrometry (Huang et al., 1999). PO_4^{3-}
867 was determined by molybdenum blue spectrophotometric method (Huang et al., 1999).
868 DO concentration in overlying water was measured by portable dissolved oxygen meter
869 (HQ40D, UAS).

870 The concentration of DIC in pore water was measured by the following method
871 (Hannides and Aller, 2016). Briefly, 2 mL filtered water was transferred through
872 syringe into a N_2 pre-flushed vial with 0.5 mL 1 M HCl sealed with a shrimp cap with
873 rubber septum. Following the acidification and shaking for 20 min, the concentration
874 of CO_2 at headspace was measured by Gas chromatography (GC7890, Agilent, USA).
875 Fe(II) in porewater and L-Fe(II) extracted from sediment was determined by ferrozine

method (Thomsen et al., 2004). 5 ml ferrozine solution containing 1% hydroxylamine hydrochloride was add to 100 μL filtered water extracted from sediment and was determined at 562 nm after 15 min static response for total Fe. The Fe(III) concentration was the difference between total Fe and Fe(II). The concentrations of SO_4^{2-} and CH_4 were measured using an ion chromatograph (ICS-2000) and a gas chromatograph (GC7890, Agilent, USA). Spectral scanning was performed with an ultraviolet-visible spectrophotometer (UV 2700, Shimadzu, Japan).

Fluorescence EEMs were scanned with a fluorescence spectrophotometer (Fluorolog-3, Horiba, Japan) at the excitation/emission wavelengths of 250-450/280-550 nm, in 5-cnm intervals/1-nm intervals. Blank EEMs and Raman scans (λ_{Ex} = 350 nm, λ_{Em} = 360-450 nm at 1nm intervals) of Milli-Q water were also collected (Murphy et al., 2013). The PARAFAC modeling was conducted in MATLAB (R2012a) using the drEEM and N-way toolbox and a total of 83 fluorescence EEM data array were obtained for the PARAFAC modeling and statistical analysis (Murphy et al., 2008). After several post-acquisition steps (i.e., scattering removal and data arrangement) for correcting the fluorescence EEM spectra, the PARAFAC models with five components were computed. The residual analysis, split half analysis, and visual inspection were applied to determine the correct numbers of components (Stedmon and Bro, 2008).

In PE study, following the acidification (0.5 ml 1M HCl), the headspace $\delta^{13}C$-$\sum CO_2$ were measured using a isotope ratio mass spectrometer (MAT 253plus，Thermo Finnigan, USA). Total $\sum CO_2$ was the sum of that measured directly in the slurry bottle

gas-phase and liquid-phase upon acidification. Carbon isotopes are expressed in the delta notation ($\delta^{13}C$) relative to Vienna Pee Dee Belemnite.

Text S4 Characterization of dissolved organic matter

Using the EEM-PARAFAC, five DOM components (C1-C5) were obtained in our study (Fig. S1, Table S3). Compared with those identified in other aquatic ecosystems (Murphy et al., 2013), C1 was similar to a microbial humic-like fluorophore and generally considered to be associated with biological activitcies or eutrophication. C2 could be classified as tryptophan-like substances that was traditionally considered to come from autochthonous compounds. C3 was characterized as humus associated with UVA compounds. C4 was also a type of humic-like which was similar to that of marine-humic materials. C5 basically fell in the range of the terrestrial fluorescent component defined by Coble (1996) (Coble, 1996), as it was primarily observed in the open ocean environment. C1 was accounted for nearly a half of the total fluorescence intensities in the ×20 amended treatment but decreased over time and lower than that of the control at the end of the cultivation. The relative contribution of the components of C2 and C3 in the ×20 amended treatment was also decreased during cultivation. Thus, the contribution of C4 and C5 increased at the end of experiment, indicating that SOM composition was dominated by humus and unstable AOM has been abundantly transformed into refractory organics.

Table S1 Characteristics of algal debris and sediments.

Sample	C (%)	N (%)	C/N	δ^{13}C-OM	δ^{13}C-carbonate	Chl-a (ug/g)	Wet Weight (g)
Sediment	3.91	0.60	6.52	-14.5‰	0.50	0.43	12.38
Algal-debris	35.41	3.65	9.70	28.9%	--	3136	--

Table S2 Accumulation rates (μmol·L^{-1}·d^{-1}) of DIC and NH_4^+-N of different sediment depths in the various treatments during bag incubations.

Depth-range (cm)	DIC (μmol·L^{-1}·d^{-1})			NH_4^+-N (μmol·L^{-1}·d^{-1})		
	Control	×1 amendment	×20 amendment	Control	×1 amendment	×20 amendment
0–1	49.92 ± 2.84	18.16 ± 3.93	168.60 ± 2.76	5.03 ± 0.00	1.45 ± 0.05	18.11 ± 2.33
1–2	25.43 ± 0.84	31.00 ± 8.45	22.52 ± 6.70	3.45 ± 0.49	0.98 ± 0.32	4.31 ± 0.52
2–3	7.15 ± 3.82	8.09 ± 3.16	10.58 ± 2.31	0.26 ± 0.09	0.61 ± 0.07	0.50 ± 0.15
3–4	12.31 ± 2.08	30.04 ± 3.73	16.97 ± 1.17	0.09 ± 0.01	0.24 ± 0.05	1.24 ± 0.75
4–6	11.01 ± 1.54	24.66 ± 1.61	5.80 ± 0.68	0.94 ± 0.03	0.61 ± 0.17	5.18 ± 0.59
6–8	2.55 ± 0.42	8.90 ± 0.07	1.05 ± 0.07	2.38 ± 0.04	2.73 ± 0.08	9.01 ± 1.67

R^2: the coefficient of linear regression between the concentration of DIC or NH_4^+-N and incubation time.

925 **Table S3 Excitation (Ex) and emission (Em) maxima of the five PARAFAC**

926 **components and possible assignments.**

Component	Ex_{max} (nm)	Em_{max} (nm)	Classify	Source
C1	340	424	Humic-like	Microbial life activities or eutrophic water bodies(Zhou et al., 2019)
C2	280	344	Tryptophan-like	Autogenetic(Murphy et al., 2013)
C3	280/385	504	UVA humic-likec	Terrigenous and Autogenetic(Murphy et al., 2013)
C4	315	360	Marine humic-like	Microbial degradation of phytoplankton(Murphy et al., 2008; Yang et al., 2014)
C5	275/410	458	Terrestrial humic-like	Terrigenous(Zhou et al., 2019)

927

928

929

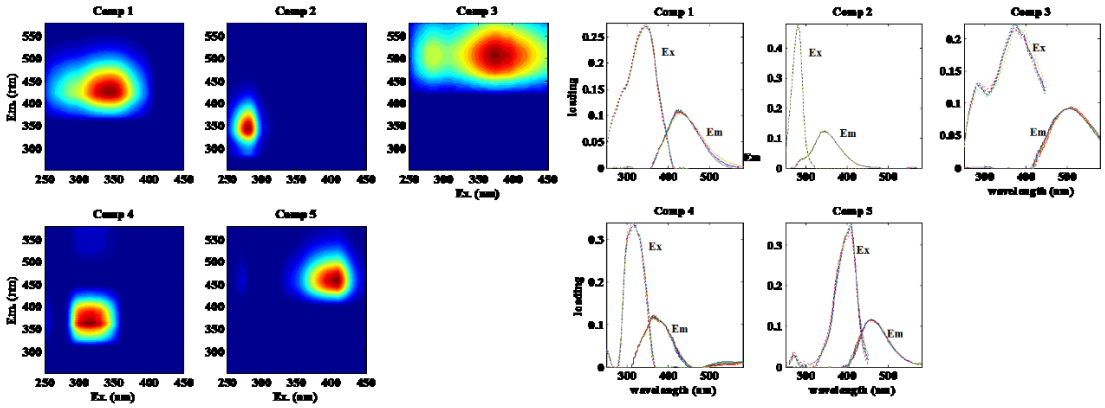

930

931

932 **Fig. S1.** EEM contours and the spectral characteristics of the EEM-PARAFAC

933 components during the bag-incubation experiment.

934

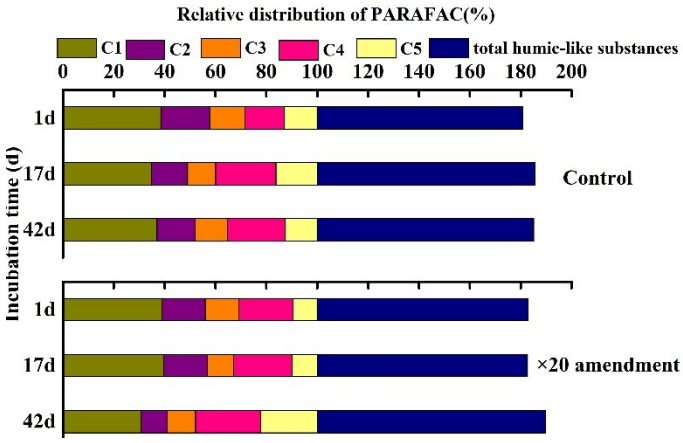

935

936

937 **Fig. S2.** The proportion of each component in DOM at the depth of 0−1 cm. Total

938 humic-like substances were the sum of C1, C3, C4, C5 during bag-incubation

939 experiment.

940

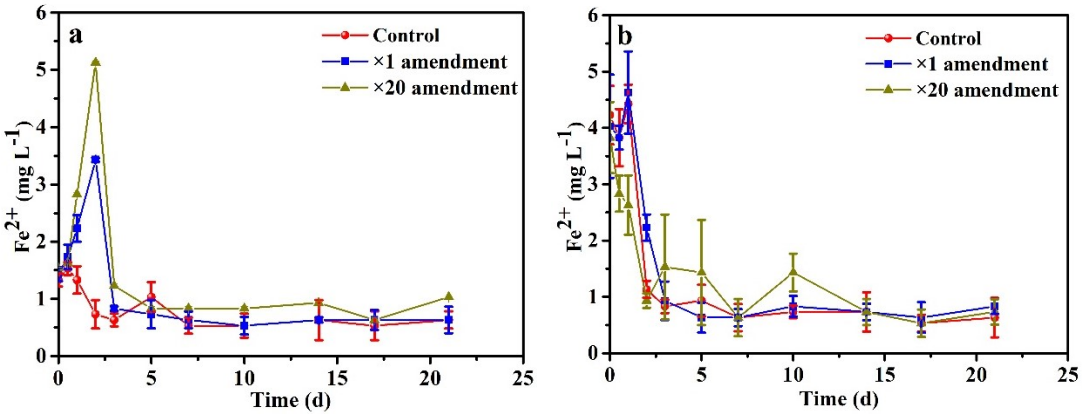

941

942

943 **Fig. S3.** Fe^{2+}concentration in overlying water (a) and pore water (b) during priming

944 effect study with different treatments.

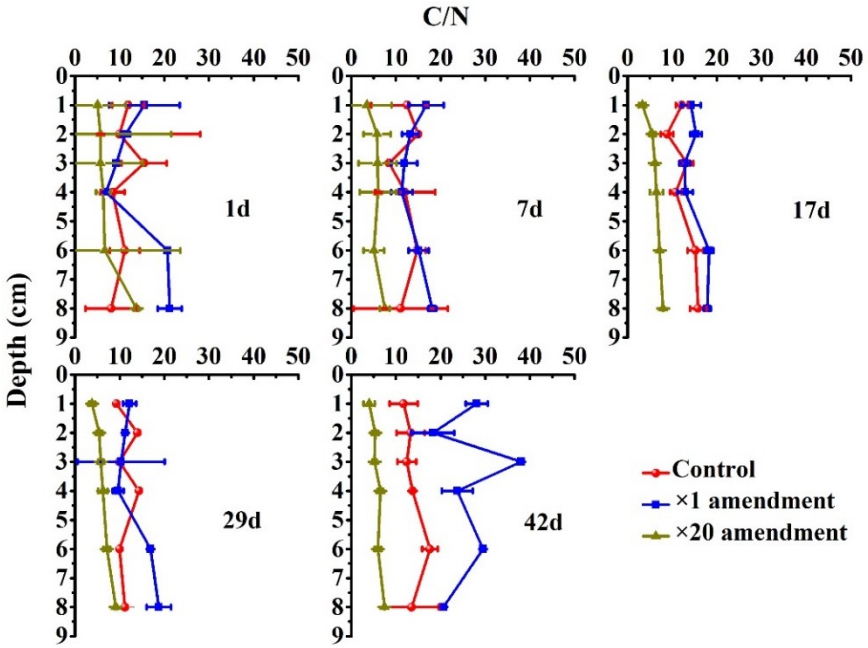

Fig. S4. The vertical distribution of C/N during bag-incubation experiment.

References

Coble, P.G., 1996. Characterization of marine and terrestrial DOM in seawater using excitation emission matrix spectroscopy. Mar. Chem. 51(4), 325–346.

Hannides, A.K. and Aller, R.C., 2016. Priming effect of benthic gastropod mucus on sedimentary organic matter remineralization. Limnol. Oceanogr. 61(5), 1640–1650.

Hou, L., Yin, G., Liu, M., Zhou, J., Zheng, Y., Gao, J., Zong, H., Yang, Y., Gao, L. and Tong, C., 2015. Effects of Sulfamethazine on Denitrification and the Associated N_2O Release in Estuarine and Coastal Sediments. Environ. Sci. Technol. 49(1), 326–333.

Huang, X.; Chen W.; Cai, Q., 1999. Analysis and Ecological Investigation of Lake. Standards Press, Beijing, 27–62.

Kana, T.M., Darkangelo, C., Hunt, M.D., Oldham, J.B., Bennett, G.E. and Cornwell, J.C., 1994. Membrane inlet mass-spectrometer for rapid high-precision determination of N_2, O_2, and Ar in environmental water samples. Anal. Chem. 66(23), 4166–4170.

Murphy, K.R., Stedmon, C.A., Graeber, D. and Bro, R., 2013. Fluorescence spectroscopy and multi-way techniques. PARAFAC. Analytical Methods 5(23), 6557–6566.

Murphy, K.R., Stedmon, C.A., Waite, T.D. and Ruiz, G.M., 2008. Distinguishing between terrestrial and autochthonous organic matter sources in marine environments using fluorescence spectroscopy. Mar. Chem. 108(1-2), 40–58.

Song, G.D., Liu, S.M., Marchant, H., Kuypers, M.M.M. and Lavik, G., 2013. Anammox, denitrification and dissimilatory nitrate reduction to ammonium in the East China Sea sediment. Biogeosciences. 10(11), 6851–6864.

Stedmon, C.A. and Bro, R., 2008. Characterizing dissolved organic matter fluorescence with parallel factor analysis: a tutorial. Limnology and Oceanography-Methods 6, 572–579.

Thomsen, U., Thamdrup, B., Stahl, D.A. and Canfield, D.E., 2004. Pathways of organic carbon oxidation in a deep lacustrine sediment, Lake Michigan. Limnol. Oceanogr. 49(6), 2046–2057.

976 Yang, L., Choi, J.H. and Hur, J., 2014. Benthic flux of dissolved organic matter from lake
977 sediment at different redox conditions and the possible effects of biogeochemical processes.
978 Water Res. 61, 97–107.

979 Zhou, Y., Zhou, L., Zhang, Y., de Souza, J.G., Podgorski, D.C., Spencer, R.G.M., Jeppesen, E.
980 and Davidson, T.A., 2019. Autochthonous dissolved organic matter potentially fuels methane
981 ebullition from experimental lakes. Water Res.166: 115048.

982

983

984